Title
Nitroxoline induces apoptosis and slows glioma growth in vivo

Journal
Neuro-Oncology, 17(1)

ISSN
1522-8517

Authors
Lazovic, Jelena
Guo, Lea
Nakashima, Jonathan
et al.

Publication Date
2015

DOI
10.1093/neuonc/nou139

Peer reviewed

Neuro-Oncology

Neuro-Oncology 17(1), 53–62, 2015
doi:10.1093/neuonc/nou139
Advance Access date 28 July 2014

Nitroxoline induces apoptosis and slows glioma growth in vivo

Jelena Lazovic, Lea Guo, Jonathan Nakashima, Leili Mirsadraei, William Yong, Hyun J. Kim, Benjamin Ellingson, Hong Wu, and Whitney B. Pope

Department of Radiological Sciences, Ronald Reagan UCLA Medical Center, Los Angeles, California (J.L., L.G., H.J.K., B.E., W.B.P.); Department of Molecular and Medical Pharmacology, David Geffen School of Medicine at UCLA, University of California at Los Angeles, Los Angeles, California (J.N., H.W.); Department of Pathology, University of California San Diego Medical Center, San Diego, California (L.M.); Department of Pathology and Laboratory Medicine, David Geffen School of Medicine at UCLA, University of California at Los Angeles, Los Angeles, California (W.Y.); Department of Biostatistics, Fielding School of Public Health and Department of Radiological Sciences, David Geffen School of Medicine at UCLA, Los Angeles, California (H.J.K.)

Corresponding Author: Whitney B. Pope, PhD, Department of Radiological Sciences, UCLA Radiology Sciences, 757 Westwood Blvd., Ronald Reagan UCLA Medical Center, room #1621E, Los Angeles, CA 90095 (wpope@mednet.ucla.edu).

Background. Nitroxoline is an FDA-approved antibiotic with potential antitumor activity. Here we evaluated whether nitroxoline has antiproliferative properties on glioma cell growth in vitro and in vivo using glioma cell lines and a genetically engineered *PTEN/KRAS* mouse glioma model.

Methods. The effect of nitroxoline treatment on U87 and/or U251 glioma cell proliferation, cell-cycle arrest, invasion, and ability to induce an apoptotic cascade was determined in vitro. Magnetic resonance imaging was used to measure glioma volumes in genetically engineered *PTEN/KRAS* mice prior to and after nitroxoline therapy. Induction of apoptosis by nitroxoline was evaluated at the end of treatment using terminal deoxyribonucleotidyl transferase (TDT)-mediated dUTP-digoxigenin nick end labeling (TUNEL).

Results. Nitroxoline inhibited the proliferation and invasion of glioblastoma cells in a time- and dose-dependent manner in vitro. Growth inhibition was associated with cell-cycle arrest in G_1/G_0 phase and induction of apoptosis via caspase 3 and cleaved poly(-ADP-ribose) polymerase. In vivo, nitroxoline-treated mice had no increase in tumor volume after 14 days of treatment, whereas tumor volumes doubled in control mice. Histological examination revealed 15%–20% TUNEL-positive cells in nitroxoline-treated mice, compared with ~5% in the control group.

Conclusion. Nitroxoline induces apoptosis and inhibits glioma growth in vivo and in vitro. As an already FDA-approved treatment for urinary tract infections with a known safety profile, nitroxoline could move quickly into clinical trials pending confirmatory studies.

Keywords: glioma animal model, invasion, nitroxoline, PTEN, 8-hydroxy-5-nitroquinoline.

The development of more effective therapeutic agents for high-grade gliomas remains a major challenge in neuro-oncology. Even with state-of-the-art surgical techniques, radiation, and temozolomide treatment, the median survival for the most aggressive gliomas (grade IV, glioblastoma) is 12–16 months from diagnosis and has improved little over the past 10 years.[1,2] The ultimate failure of available treatments is attributed to drug resistance, infiltrative properties of high-grade gliomas, and the inability to completely resect invading tumor cells. Molecular mechanisms that enable glioma cells to resist apoptosis, ultimately leading to treatment failure, are only partially elucidated. Glioma cells have unique properties that enable them to break down the extracellular matrix and invade adjacent brain parenchyma. The expression of plasminogen activators, matrix metalloproteinases, and cysteine proteases all correlate with glioma progression, grade, and more invasive phenotype. For these reasons, more effective therapeutic agents could be sought among the compounds that can efficiently induce apoptosis while inhibiting tumor cell invasion. Recently, the FDA-approved antibiotic 8-hydroxy-5-nitroquinoline (nitroxoline) has regained attention due to its more potent anticancer properties than similar compounds that are also structurally related to clioquinol and 8-hydroxyquinoline.[3] Nitroxoline was found to be one of the most effective inhibitors of angiogenesis and type 2 methionine aminopeptidase (MetAP2) among 175 000 compounds from a library of FDA-approved drugs.[4] The same study demonstrated nitroxoline's ability to significantly inhibit growth of breast and bladder

Received 15 January 2014; accepted 23 June 2014

cancer xenografts in vivo.[4] Apart from its role in the inhibition of angiogenesis, nitroxoline was recently shown to inhibit expression of cysteine proteinase cathepsin B (catB).[5,6] CatB is elevated in many neoplasms including melanoma and breast, lung, ovarian, colorectal, and brain cancers.[7,8] High levels of catB are found at the invasive edge of anaplastic astrocytomas and glioblastoma and in their cell culture media.[9] Therefore, as a compound with the potential to suppress glioma invasion, nitroxoline has several advantages including a long history of human use (having been prescribed for urinary tract infections for more than 50 years in Europe[10]), tolerable side effects, and a favorable pharmacokinetic profile. As an already FDA-approved drug, nitroxoline has the potential to quickly enter clinical trials as an anticancer agent if it is shown to be effective for specific tumor types.

Animal models that faithfully mimic the glioma microenvironment are necessary to evaluate drug therapies. Orthotopic xenograft models that use glioma/glioblastoma-derived cell lines have been commonly used for interventional studies, but their clinical relevance is questionable because of the inability to recapitulate many of the features that characterize high-grade gliomas. Several novel tumor models that more closely mimic human gliomas have been recently introduced.[11–13] In the current work, we employ a genetically engineered mouse model based on adult neural stem cell-specific phosphatase and tensin homolog (*PTEN)* deletion and overexpression of human Kirsten rat sarcoma viral oncogene homolog $KRAS^{G}12^{D}$ capable of recapitulating many of the characteristics of human glioma. This glioma model was combined with magnetic resonance imaging (MRI) to evaluate treatment efficacy and help develop MRI biomarkers that can be used to monitor and predict treatment response to nitroxoline.

Methods

Cell Lines and Culture

U87 and U251 glioblastoma cells (obtained from Dr. Paul Mischel, formerly at UCLA) were cultured in Roswell Park Memorial Institute (RPMI)-1640 medium (Invitrogen) or Dulbecco's Modified Eagle's Medium (DMEM) medium supplemented with 10% fetal bovine serum (FBS), 2 mM glutamine, and 100 units/mL of penicillin/streptomycin. Human lung adenocarcinoma A549 cell line (obtained from Dr. David Shackelford, UCLA) and human prostate cancer cell line PC3 (obtained from Dr. Hong Wu, UCLA) were cultured in RPMI medium supplemented with 10% FBS and 100 units/mL of penicillin/streptomycin.

Cytotoxicity Assay

A cell counting kit-8 (CCK-8, Dojindo) was used to determine cell viability following nitroxoline (Sigma-Aldrich) treatment. Four different human cancer cell lines (glioblastoma U87 and U251, lung adenocarcinoma A549, and prostate cancer PC3) were plated in triplicate in 96-well plates, 5000 cells per well. Cells were incubated in RPMI medium containing 1% dimethyl sulfoxide (DMSO) (control) or 20, 40, 60, 80, and 100 μg/mL nitroxoline (dissolved in DMSO) for 24 hours at 37°C. After incubation with nitroxoline/DMSO, cells were washed 3 times with phosphate-buffered saline (PBS) and incubated with CCK-8 for 2 hours at 37°C. The amount of formazan formed by viable cancer cells was determined by absorbance at 450 nm using the Synergy H1 plate reader. The amount of viable cells for different nitroxoline concentrations was expressed as a percentage of control cells. All treatment conditions were done in triplicate. Concentration response course analysis was performed (Sigma Plot 12.5 software, Jandel Scientific) to determine nitroxoline concentrations required to inhibit the growth of cancer cells by 50% (IC_{50}) after incubation for 24 hours.

Cell-cycle Analysis by Flow Cytometry

U87 cells (1×10^5) were plated in 12-well plates and treated with nitroxoline (5, 10, and 20 μg/mL) in DMEM supplemented with 5% FBS for 24 hours. Cells were trypsinized with TrypLE Express (Invitrogen) and washed once with PBS. Cells were stained with solution containing sodium citrate, 1% Triton x-100, propidium iodide, and 0.1 mg/mL ribonuclease A for 30 minutes on ice. Separation of cells in G0/G1, S, and G2/M was based on DNA content (fluorescence intensity) after staining with propidium iodide. Cells were analyzed using BD LSRII flow cytometer, and the percentage of cells in each phase of cell cycle was obtained using Modfit Software (Varity Software House).

Western Blotting

U87 cells (2×10^5 cells) were seeded onto 6-well plates in RPMI medium one day before nitroxoline treatment (0, 20, 40, and 60 μg/mL). Cells were collected after 24 hours of incubation and lysed in boiled sodium dodecyl sulfate (SDS)-lysis buffer (10 mM tris [pH 7.5],100 mM NaCl, 1% SDS, and protease inhibitor cocktail). Each lane was loaded with 15 μg of protein and resolved on 4%–12% Bis-Tris NuPAGE (Invitrogen). After electrophoresis, proteins were transferred onto PVDF membrane and probed with specific antibodies. (For a full list, please see Supplementary methods.) Proteins were detected by ECL-Plus and scanned on a Typhoon 9400 scanner. Relative band intensities were measured by densitometry.

U87 Cell Invasion Assay

Two hours prior to invasion assay, 24-well chambers (353097, BD Biosciences) were coated with 300 μg/mL of Matrigel (356234, BD Biosciences) according to the manufacturer's instructions. Cell suspensions containing 1×10^5 U87 cells (in DMEM medium) were added to each chamber. DMEM with 5% FBS was added to the lower chamber as a chemoattractant. After 24 hours of incubation, noninvading cells were removed with cotton swabs, and cells were fixed in methanol for 5 minutes. Cells were then stained in 0.2% crystal violet solution for 20 minutes and washed in 3 changes of water. After air-drying, cells were destained with 200 μL of 10% acetic acid, and 150 μL aliquot was transferred to a 96-well plate and counted on a Synergy H1 Hybrid Multi-mode Reader (Biotek) at absorbance 590 nm. Since the absorbance value of crystal violet directly correlates with the number of stained cells, we used this correlation to calculate the percentage of invasion. The percent of invading cells was calculated by dividing mean absorbance value of stained cells invading through BD Matrigel

matrix insert membrane with mean absorbance value of cells migrating through uncoated insert membrane and multiplying by 100.

Genetically Engineered Mouse Glioma Model

All animal experiments were approved by our institution's Animal Care and Use Committee. For the in vivo evaluation of nitroxoline as a potential antiglioma compound, we used a *mGFAP-Cre+*; *PTEN* $^{lox/lox}$; *LSL-KRAS* $^{G12D/+}$ mouse model (*PTEN/KRAS* in short*)* generated by Dr. Hong Wu at UCLA. Conditionally expressed *PTEN* $^{lox/lox}$; *LSL-KRAS* $^{G12D/+}$ leads to spontaneous development of grade III glioma between 6 and 8 weeks of age. Previously, we reported that deletion of *PTEN* in adult neural stem cells of the subventricular zone enhances constitutive neurogenesis without the onset of tumorigenesis.[14] Here we introduced a new model by conditionally deleting *PTEN* with concomitant overexpression of human Kirsten rat sarcoma viral oncogene homolog KRAS (G12D). (For more information on *PTEN/KRAS* glioma model, please see Supplementary material.)

Magnetic Resonance Imaging

MR imaging was performed on a 7T Bruker system with a custom-built 2.2 cm RF birdcage coil. *PTEN/KRAS* mice were imaged between 10 and 12 weeks of age to determine presence of glioma. If glioma was confirmed on T_2-weighted image, the mouse was randomly assigned to nitroxoline ($n = 6$ mice total) or control group (soybean oil, $n = 6$ mice total). The MR imaging was repeated after 7 and 14 days. Mice assigned to the nitroxoline group were injected intraperitoneally with 80 mg/kg nitroxoline (pharmaceutical grade, MIP Pharma) suspended in soybean oil every day for 14 days. Control groups received daily 0.01 mL/g soybean oil injections. Animals were anesthetized with isoflurane (4% induction, maintenance with 1.5%). Mice were kept warm with water heated to 37°C and circulated using a water pump (Gaymar Solid State TP500). The tumor volume was determined from T_2-weighted imaging sequence (TR/TE_{eff} = 6000/93.87, 78 μm^2 inplane resolution, 1 mm slice thickness, NEX = 8) by multiplying the slice thickness and the tumor area. A semiautomated routine based on signal intensity threshold segmentation was used to calculate the tumor area by an investigator blinded to the treatment groups. To quantify transverse relaxation time T_2, a multislice multi-echo (MSME) spin-echo sequence was used (TR/TE = 2000/7.26–101.64 ms, 14 echoes, 78 μm^2 inplane resolution, 1 mm slice thickness, NEX = 2). A diffusion-weighted echo planar imaging (DWI-EPI) sequence (TR/TE = 3800/22.03 ms, with 3 b-value = 0, 500, 1000, 3 diffusion directions and 156^2 μm^2 resolution, 1 mm slice thickness, NEX = 2) was used to calculate apparent diffusion coefficient (ADC). Nonlinear least-squares regression was used to estimate ADC from multiple b-value DWIs and T_2 from MSME data on a voxel-wise basis. The ADC and T_2 values were calculated as a mean from each tumor region of interest. Following all other MRI pulse sequences, a postcontrast T1-weighted spin-echo dataset (1 mm thick slices, TR/TE 500/7.3 ms, 78 μm^2 resolution, NEX = 2) was acquired using 0.05 mL Gd-DTPA i.v. injection to visualize blood-brain barrier (BBB) compromise. All MRI data processing was done using the NIH software ImageJ (rsbweb.nih.gov/ij/).

Histology, Immunohistochemistry, and Terminal Deoxynucleotide Transferase-mediated dUTP Nick-end Labeling Staining

At the end of MRI studies, all animals were overdosed with 100 mg/kg pentobarbital and perfused with 10% formalin. The brain tissue was extracted and paraffin embedded using standard procedures. Sections (5-μm thick) were cut, deparaffinized, and stained by standard hematoxylin and eosin (H&E) technique. H&E sections were examined by a neuropathologist (W. Y) to confirm the presence of glioma. Identified gliomas were graded using WHO histopathological criteria: nuclear atypia, mitotic index, necrosis, and microvascular proliferation. Adjacent sections were processed for vascular endothelial growth factor (VEGF) immunohistochemistry using mouse monoclonal antibody (1 : 200) (Santa Cruz Biotechnology), followed by Dako Envision+ system (peroxidase) with blocking steps and secondary antibody dilutions according to the manufacturer's instructions (DakoCytomation). Sections obtained from U87 orthotopic xenograft model (5-μm thick) were processed as a positive control for VEGF. NovaRED (Vector Laboratories) was used as a chromogen. Mayer's hematoxylin was used as a counterstain. Additional adjacent sections were TUNEL stained (2 sections from each animal) using the DeadEnd Colorimetric TUNEL system (Promega) followed by exposure to chromogen, diaminobenzidine (DAB), and hematoxylin for counterstaining. TUNEL-positive cells were counted by a pathology resident (L. M.) blinded to the experimental design. A score between 0 and 4 was assigned for each section: 0 for no TUNEL-positive cells; 0.5: for 1%–5%; 1: for 6%–10%; 2: for 11%–30%; 3: for 31%–50%; and 4 for $>$ 50% TUNEL-positive cells. The averaged score from 2 sections was calculated.

Statistical Analysis

One-way analysis of variance (ANOVA) with the Dunnett' post hoc test was used to analyze data from the nitroxoline cytotoxicity assay, cell cycle, and U87 cell invasion assays. Western Blot data were analyzed using 1-way ANOVA on ranks with the Dunnett' post hoc test. A 2-way ANOVA with repeated measures was performed, where changes in volume from day 0 were considered outcome, and the treatment group and duration of days (7 and 14) were 2 factors. Trend tests were performed within each group to test for an increase or decrease in tumor volume over day 0 (pretreatment) and days 7 and 14 (posttreatment). A mixed-effects maximum likelihood regression with random intercept and slope model was used to consider the dynamic changes over days in which the dependent variable was the change in volume. The fixed effects were treatment and days, and the random effect was the individual mouse. Box-Cox transformation was used for the ADC analysis, and the similar mixed-effects regression model was used to account for motion artifact from ADC measurements. A 2-sample *t* test was used to compare TUNEL scores between *PTEN/KRAS* gliomas and the control group in vivo. Sigma Plot 12.5 software (Jandel Scientific) and STATA 12.0 were used for analysis.

Results

Dose and Time Response for the Antiproliferative Effect of Nitroxoline on Human Cancer Cell Lines in Vitro

The potential of nitroxoline to inhibit cell proliferation for human glioblastoma cell lines (U87 and U251) was first investigated in vitro and was compared with growth inhibitory effects on 2 other human cancer cell lines: lung adenocarcinoma (A549) and human prostate cancer cells (PC3). At 24 hours, we found a significant dose-response inhibition of glioblastoma cell growth with nitroxoline concentration ranging from 5–80 μg/mL for U251 cells and 40–100 μg/mL for U87 cells, (Fig. 1A). A similar dose response was found with human lung adenocarcinoma cells (A549) and prostate cancer cells (PC3) (Fig. 1A). Nitroxoline was most toxic to U251 glioblastoma cells, with significant inhibition of growth starting at a 5 μg/mL concentration, (Fig. 1A). The half-maximal inhibitory concentration (IC_{50}) of nitroxoline was lowest for the U251 cell line and highest for the U87 glioblastoma cell line (Table 1). Analysis of time-dependent response revealed that nitroxoline was effective as early as 4 hours at significantly inhibiting proliferation of U251 cell line starting at a 10 μg/mL concentration (Fig. 1B–D). In contrast to this rapid response for U251 cells, nitroxoline became an effective inhibitor of U87 cell proliferation at 24 hours starting at a concentration 60 μg/mL (Fig. 1B–D). Because the U251 glioma cell line was very sensitive to nitroxoline, we used U87 cells to determine if nitroxoline could lead to cell-cycle arrest and induce apoptosis.

Cell-cycle Arrest in U87 Cells Following Nitroxoline Treatment

To investigate the mechanism by which nitroxoline inhibits growth, we performed cell-cycle analysis on U87 cells. Following propidium iodine staining, fluorescence-activated

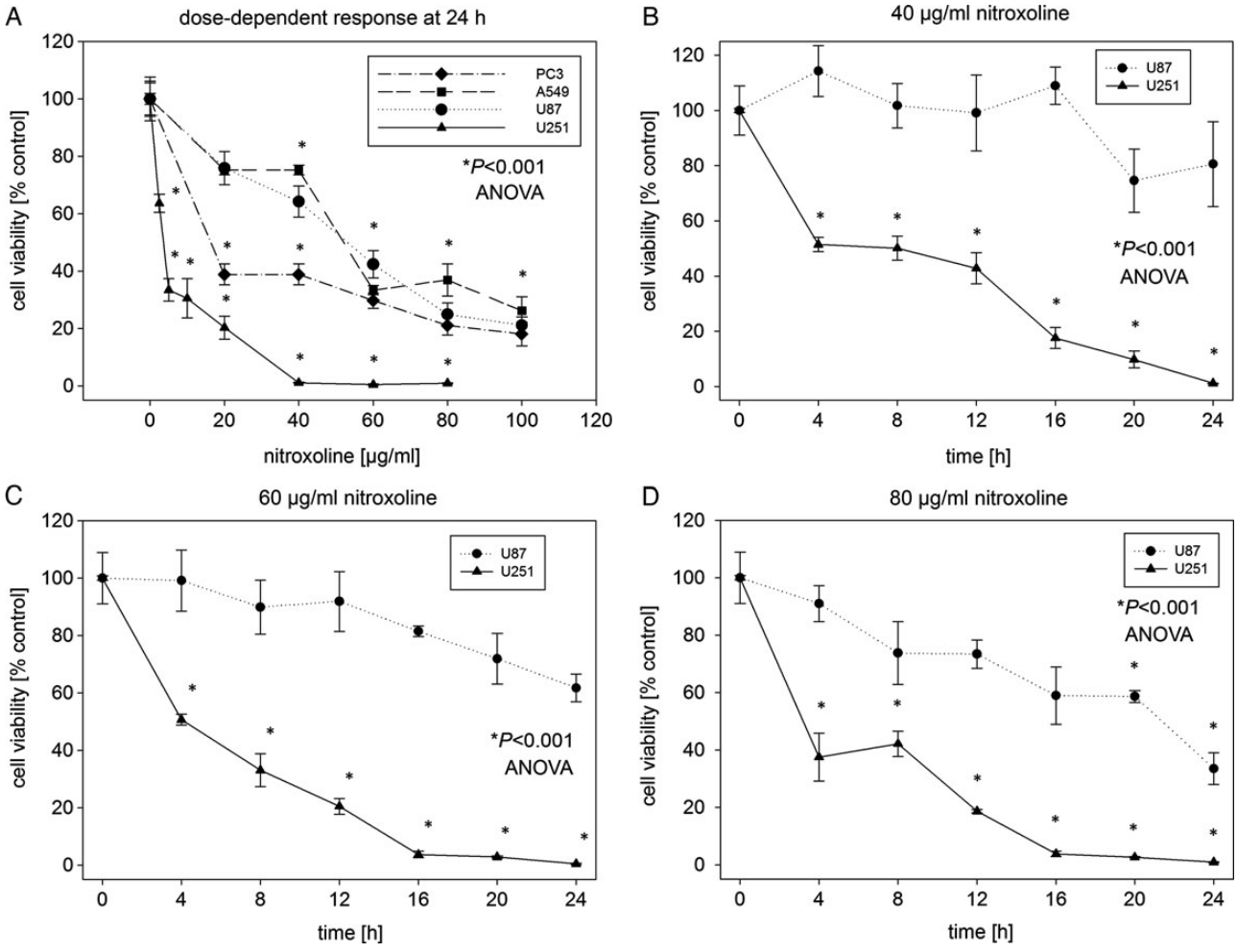

Fig. 1. (A) Dose-dependent inhibition by nitroxoline of U87, U251, PC3, and A549 cell proliferation. Viable cells were quantified by CKK-8 assay after 24 hours of culturing in the presence of different concentrations of nitroxoline. The mean of the absolute absorbance values given by nitroxoline-treated cells was divided by the mean of the absolute absorbance of control-treated cells and expressed as the percent of viable cells. Data are represented as mean ± SEM of 4 independent experiments. Time-dependent inhibition of U87 and U251 cell proliferation following 40 μg/mL (B), 60 μg/mL (C), and 80 μg/mL (D) of nitroxoline is shown. Statistical analysis was done using 1-way ANOVA with Dunnett' post hoc test (*$P < .001$).

Table 1. The half-maximal inhibitory concentration of nitroxoline for human cancer cell proliferation. Among human cell lines tested, U251 glioblastoma cell are the most sensitive to nitroxoline, while U87 glioblastoma cells are the least sensitive.

Cancer Cell Line	IC_{50} [μg/mL]
U87	50
U251	6
A549	38
PC3	23

cell sorting analysis was performed on U87 cells treated with nitroxoline. Representative cell-cycle profiles are shown in (Fig. 2). In the control group, a predominant number of U87 cells were found in G_0/G_1 and S phase. A substantial proportion of cell-cycle arrest in the G_0/G_1 phase was observed with the lowest dose of nitroxoline tested (5 μg/mL), suggesting that nitroxoline can override the bypass of the G1/S checkpoint and induce cell-cycle arrest. A similar trend of cell-cycle distribution was further observed with 10 and 20 μg/mL nitroxoline concentrations. Taken together, these results indicate a cytostatic effect of nitroxoline at doses as low as 5 μg/mL (Fig. 2).

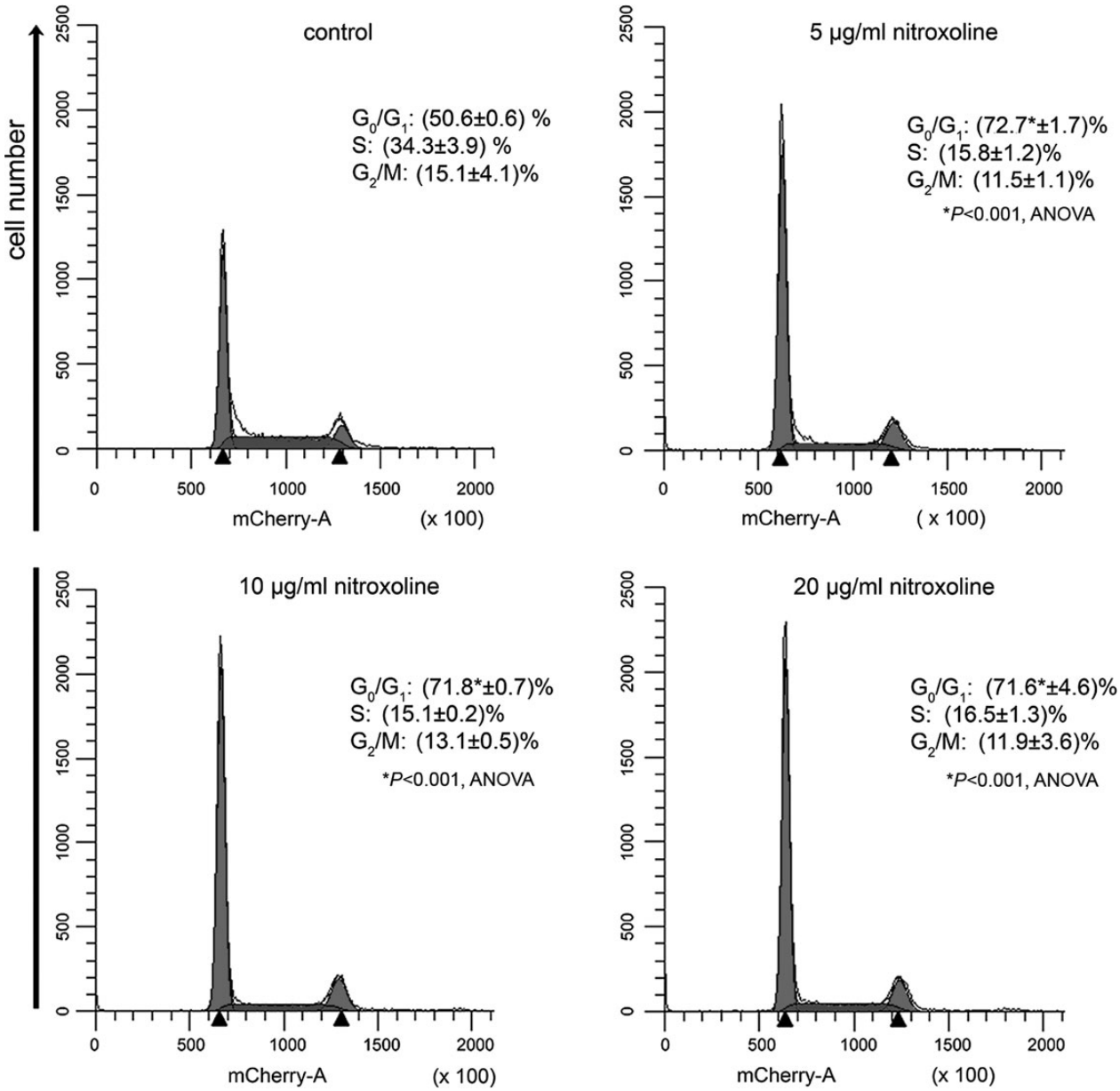

Fig. 2. Effect of nitroxoline on cell-cycle analysis. Cellular DNA content was measured by propidium iodide staining using fluorescence activated flow cytometry. (A) Control U87 cells (1×10^5) were plated and grown in DMEM media with addition of solvent only (0.1% DMSO). (B–D) The same amount of U87 cells cultured with DMEM with the addition of 5, 10, and 20 μg/mL nitroxoline for 24 hours. The percentages of cell-cycle phases (data shown as mean ± SD, $^*P < .001$, 1-way ANOVA with Dunnett' post hoc test) shown in each panel are representative of 4 independent experiments.

Induction of Caspase 3 Expression and Anti-Poly-(ADP-ribose) Polymerase Cleavage by Nitroxoline Treatment

Failure of chemotherapeutic agents to induce apoptosis in cancer cells is believed to be one of the major mechanisms underlying treatment resistance.[15,16] To differentiate between growth arrest and inhibition of proliferation versus ability of nitroxoline to induce apoptosis, we measured levels of caspase 3 and cleaved anti-poly-(ADP-ribose) polymerase (PARP) by Western blotting in U87 cells. Proteolytic cleavage of PARP by caspase 3 is a hallmark of apoptosis. We found a significant increase in caspase 3 and cleaved PARP after 24 hours of 40 and 60 μg/mL nitroxoline treatments (Fig. 3, $P = .011$ for PARP and $P = .038$ for caspase 3; 1-way ANOVA on ranks). A lower dose of nitroxoline (20 μg/mL for 24 h) did not lead to significant increase in caspase 3 and cleaved PARP, although this dose induced G_0/G_1 cell-cycle arrest. These data suggest that lower doses of nitroxoline may be cytostatic, whereas higher doses are required for induction of apoptosis.

Reduced Invasion of U87 Cells Following Nitroxoline Treatment

Malignant glioma cells have unique abilities to remodel the extracellular matrix in the central nervous system and to migrate beyond the visible borders of the tumor. Nitroxoline was previously shown to be a potent inhibitor of catB dipeptidyl carboxypeptidase activity.[5,6] CatB is a proteinase associated with invasive properties of many human cancers. Here we tested if nitroxoline could directly influence the invasive properties of U87 cells in a dose-dependent manner. Using an in vitro Matrigel invasion assay, we found significantly reduced invasion of U87 cells following 24 hours of nitroxoline treatment starting at doses as low as 10 μg/mL, which is 5 times lower than the IC_{50} (Fig. 4; $P = .038$, 1-way ANOVA with a Dunnett' post hoc test, Fig. 4B). Since we did not observe a statistically significant reduction in proliferation of U87 cells with 20 μg/mL (Fig. 1), it is unlikely that reduction in invasion is due to cell death. At lower doses of nitroxoline (2.5 and 5 μg/mL), there appeared to be a slight reduction of U87 cell invasion at 24 hours, but this was not significant, (Fig. 4; $P = .127$, 1-way ANOVA).

Effect of Nitroxoline on the Growth of Grade III Glioma In Vivo

After demonstrating the effects of nitroxoline on glioblastoma cell growth in vitro, we tested the ability of nitroxoline to inhibit glioma growth in vivo in a genetically engineered mouse glioma model. *PTEN/KRAS* mice spontaneously developed grade III glioma at 6–8 weeks of age in the white matter near the

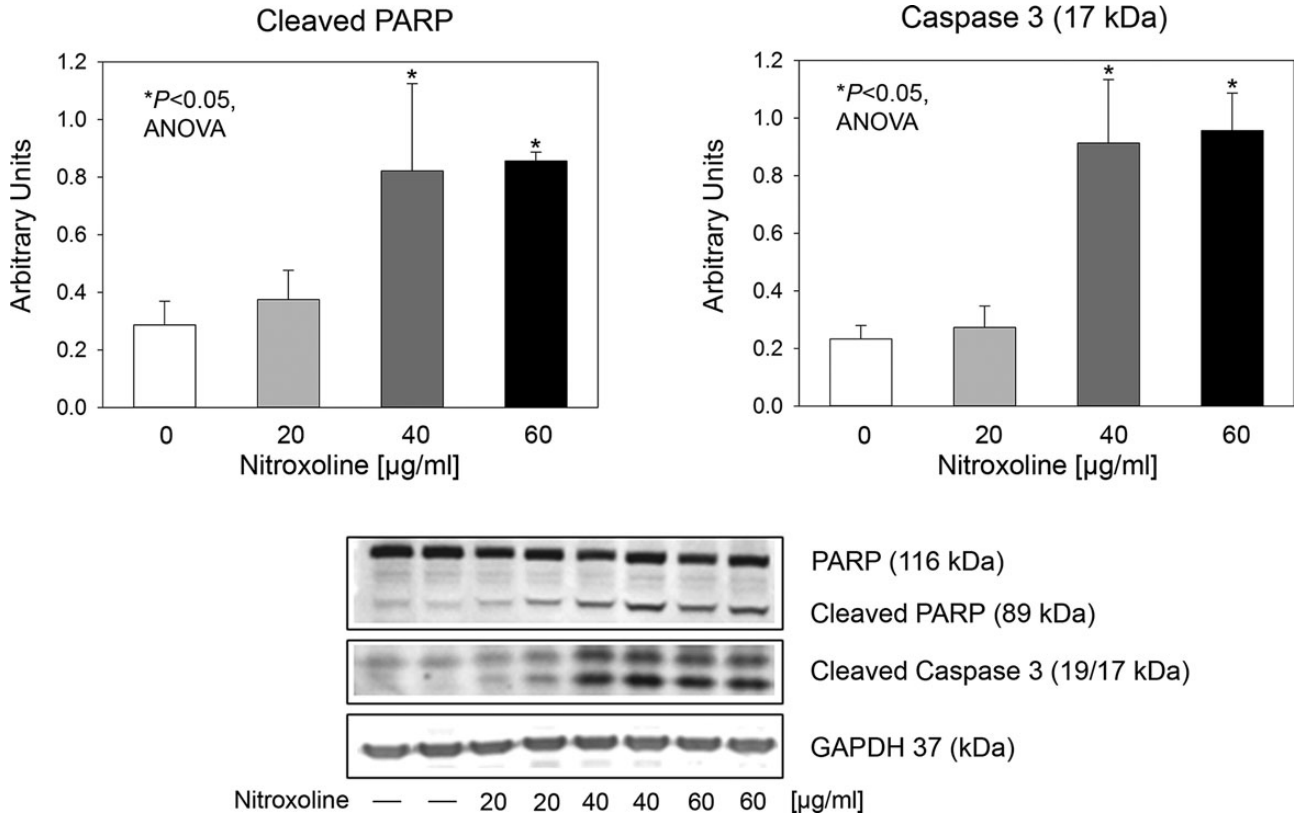

Fig. 3. Nitroxoline leads to expression of caspase 3 and PARP cleavage in U87 cells. Cells (2×10^5) were cultured in DMEM in the presence of solvent (0.1% DMSO) only (control), or increasing nitroxoline concentrations (20, 40, and 60 μg/mL) for 24 hours. Cell lysates were analyzed by Western blot for caspase 3 and PARP expression using specific antibodies that recognize both cleaved and uncleaved PARP. To account for small differences in lane loading, membranes were reprobed with GAPDH. Data are represented as mean ± SD of 4 independent experiments. Statistical analysis was performed using 1-way ANOVA on ranks with Dunnett' post hoc test (*$P < .05$).

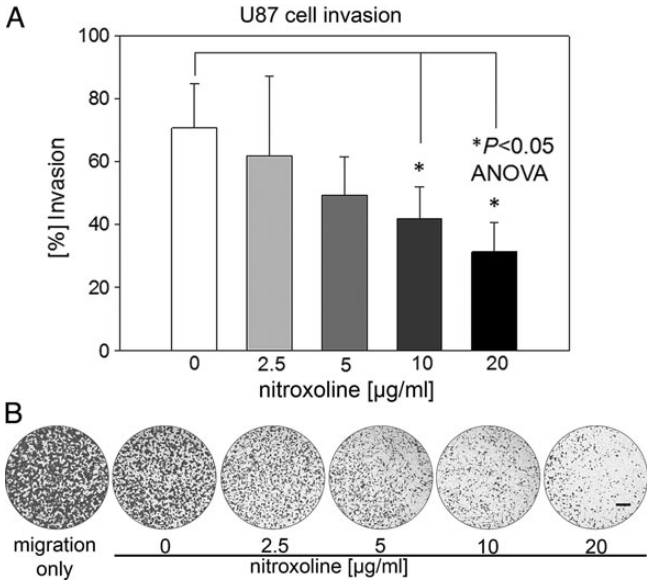

Fig. 4. (A) Effect of increasing nitroxoline concentrations (2.5, 5, 10, and 20 μg/mL) on U87 cell invasion by Matrigel invasion assay. The percent of invading cells was calculated as the mean number of cells that invaded through the Matrigel-coated membrane insert (8 μm pore size) with mean number of cells that freely migrated through the uncoated membrane insert, multiplied by 100. Data are represented as mean ± SD of 3 independent experiments. Statistical analysis was done using 1-way ANOVA with Dunnett' post hoc test (*$P < .05$). (B) Representative photographs of migrating and invading U87 cells during 24-hour incubation with nitroxoline. Scale bar represents 400 μm.

subventricular zone. By 10 weeks of age, tumors could be observed invading into the adjacent brain parenchyma. MRI was used to establish the presence of intracranial tumors and to measure the initial tumor volumes prior to nitroxoline treatment. A significant difference in volumes was found between the control and nitroxoline-treated groups at day 0, (Fig. 5M and N; $P = 0.004$). A significant increase in tumor volume was found in the control (soybean oil-treated) mice with mean (± standard deviation [SD]) change in volume of 1.68 mm^3 (±1.09) and 3.39 mm^3 (±2.03) after 7 and 14 days, respectively (Fig. 5I–L, Fig. 5M; $P = .024$ by trend test). In contrast, a slight decrease or stable tumor volume was found for the nitroxoline-treated group after 7 and 14 days of treatment (Fig. 5A–H, Fig. N; $P = 0.67$ by trend test). To investigate additional MR parameters that might correlate or predict nitroxoline treatment effect, T_2 and ADC quantification was done on tumor regions of interest. T_2 times were unchanged in the control and nitroxoline-treated groups at 7 and 14 days (Fig. 5O). In contrast, mean (±SD) ADC values were significantly increased by 0.07 (±0.10) and 0.10 (±0.09) 10^3 mm^2/s in the nitroxoline-treated cohort after 7 or 14 days posttreatment initiation, respectively (Fig. 5P; $P = .0045$), whereas there was no significant change in ADC values in the control group at either 7 or 14 days (Fig. 5P; $P = .06$). Additionally, there was no gadolinium contrast enhancement of these tumors, consistent with their having an intact BBB, (Fig. 5D,H and L).

Development of Grade III Glioma Without Increased VEGF Expression in PTEN/KRAS *Mice*

Histological examination of H&E stained brain sections from *PTEN/KRAS* mice was used to confirm the presence of glioma. In all cases (control and nitroxoline-treated mice), areas with increased signal on T_2-weighted images were found to be glioma. These tumors had features common for grade III gliomas (WHO classification: increased cell density, mitotic activity, nuclear atypia, and lack of necrosis and endothelial cell proliferation [Fig. 6A and B]). Many areas could be identified where the tumors invaded the adjacent brain parenchyma (Fig. 6A), and there were no clear borders between the normal brain parenchyma and the tumors (Fig. 6A). Immunohistochemistry for VEGF, one of the key drivers of angiogenesis,[17,18] was performed. No VEGF-immunopositive cells were found in the *PTEN/KRAS* gliomas regardless of treatment status (Fig. 6C). This contrasted with the U87 orthotopic xenograft gliomas (Fig. 6D), where anti-VEGF staining was readily apparent.

Promotion of Apoptosis by Nitroxoline Treatment in PTEN/KRAS *Glioma In Vivo*

We performed TUNEL staining on brain sections to evaluate whether nitroxoline could lead to apoptosis in vivo as one of the possible mechanisms behind the observed growth inhibition in the PTEN/KRAS glioma model. Significantly more TUNEL-positive cells were found in nitroxoline-treated animals (Fig. 6E–H, Table 2) compared with controls, consistent with the ability of nitroxoline treatment to induce apoptosis in *PTEN/KRAS* gliomas in vivo ($P = .0271$, 2-sample t test).

Discussion

This study represents the first evidence suggesting that nitroxoline can act as an antiproliferative compound against malignant glioma at a clinically relevant dose. Here we demonstrated a direct antiproliferative effect and the ability to induce apoptosis in both glioblastoma cell lines and a genetically engineered glioma mouse model. We found that lower doses of nitroxoline led to G_0/G_1 cell-cycle arrest and could inhibit invasion of glioblastoma cells in a dose-dependent manner, both very desirable treatment features. In addition, nitroxoline was effective for inhibiting proliferation of human prostate cancer cells (PC3) and human lung adenocarcinoma cells (A549) in a dose-dependent manner. Because mutated *PTEN* is common for all tested cell lines except A549,[19–21] the mechanism of nitroxoline action might involve inhibition of downstream effectors of PTEN such as the Pi3K/Akt/mTOR pathway. In the absence of functional PTEN tumor suppressor protein, increased Pi3K/Akt/mTOR signaling is thought to mediate resistance to apoptosis and promote uncoordinated G_1 cell-cycle progression leading to tumorigenesis.[19,22] In support of this mechanism, we observed G_0/G_1 cell-cycle arrest following lower doses (5–20 μg/mL) of nitroxoline treatment and expression of the apoptosis markers caspase 3 and cleaved PARP at higher doses. We also found that expression of initiation factor binding protein 4EBP1, which is involved in mTOR activation, was reduced by nitroxoline treatment in U251 cells (Supplementary Fig. S1).

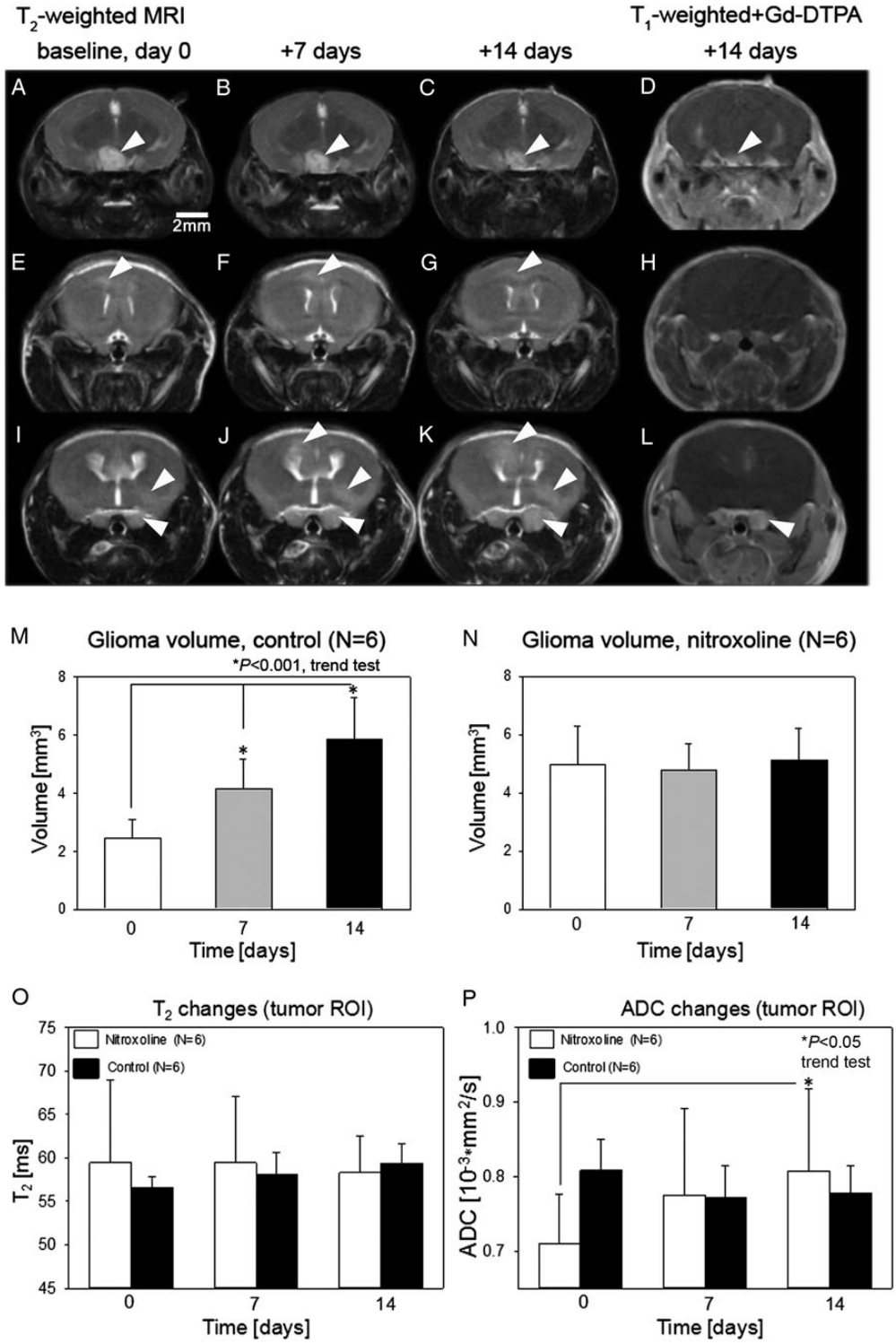

Fig. 5. Nitroxoline inhibits glioma growth in vivo. Representative T_2-weighted images before and after 7 and 14 days of 80 mg/kg nitroxoline treatment. Two different nitroxoline-treated animals are shown (A–C and E–G). Arrowheads point to the tumor location. Notice the slight reduction in tumor volume in both nitroxoline-treated animals (arrowheads). (I–K) Representative T_2-weighted images of control tumors, arrowheads point to the tumor location. (D, H, L) Notice absence of contrast enhancement on postcontrast T_1-weighted images within the tumor region of interest (arrowheads). Tumor volumes were determined before and after 7 and 14 days of vehicle (soybean oil, M) or nitroxoline (N) treatment using T_2-weighed images. Data are represented as mean ± SEM. Quantitative changes in T_2 (O) and ADC (P) values in nitroxoline-treated (n = 6) vs vehicle-treated mice (n = 6). Data are shown as mean ± SD. Statistical analysis was done using 2-way ANOVA followed by the trend test; $^*P < .001$ for glioma volume and $^*P < .05$ for ADC changes.

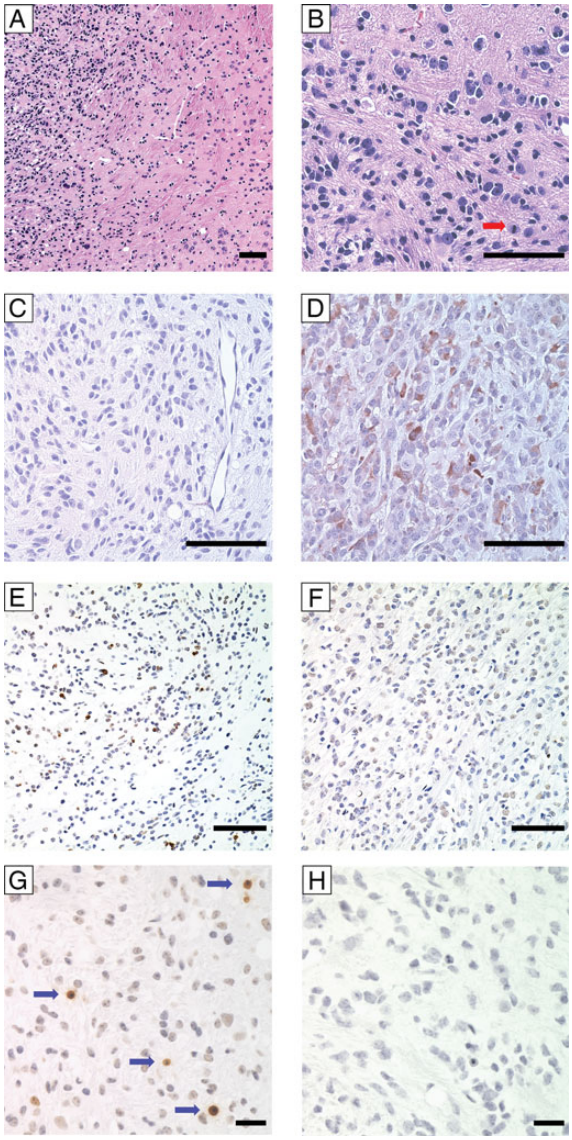

Fig. 6. H&E histology, immunohistochemistry for vascular endothelial growth factor (VEGF), and TUNEL staining in *PTEN/KRAS* mice. H&E staining shows invading glioma cells into the neighboring brain parenchyma (A). Notice absence of clear boundaries between glioma and normal brain parenchyma. Characteristics of grade III glioma: nuclear pleomorphism with mitotic nuclei (red arrow) are present (B). Immunohistochemistry for VEGF in *PTEN/KRAS* glioma (C) and U87 orthotopic xenograft as a positive control (D). Note lack of immunopositive cells in the *PTEN/KRAS* glioma specimen (C) even in the blood vessels in contrast to many VEGF immune-positive glioblastoma cells in U87 orthotopic xenografts (D). TUNEL staining showing multiple TUNEL-positive nuclei in nitroxoline-treated animal (E) versus untreated (F). Scale bar represents 100 μm. Higher magnification TUNEL staining showing TUNEL positive nuclei (blue arrows) in treated (G) animal, while no staining was present in untreated animal (H). Scale bar represents 50 μm.

According to the revised WHO classification of tumors of the nervous system,[23] about 30% of primary glioblastomas carry *PTEN* mutations. In our study, all intracranial tumors identified on MRI were confirmed by histology to be grade III glioma. None enhanced with gadolinium-DTPA on T_1-weighted images, suggesting a preserved BBB, and these tumors did not contain any VEGF-immunopositive cells that are typically associated with increased endothelial cell proliferation and angiogenesis. Supporting our in vitro findings, evidence of increased apoptosis was found in the *PTEN/KRAS* gliomas following nitroxoline treatment. Thus, it appears likely that the primary mechanism of nitroxoline action involves cell-cycle arrest and direct induction of apoptosis rather than the inhibition of angiogenesis in our model system.

Table 2. Terminal deoxynucleotide transferase-mediated dUTP nick-end labeling (TUNEL) score (mean ± SD, $^*P < .05$, 2-sample *t* test) on brain sections from control and nitroxoline-treated PTEN/KRAS mice. Two consecutive 5 μm thick sections were stained for TUNEL and scored by a pathology resident blinded to the treatment groups.

Treatment Group	Mean TUNEL Score	No. of Animals Used
Control	0.5 ± 0.0	6
80 mg/kg nitroxoline	1.625* ± 1.1	6

Abbreviation: SD, standard deviation

To help establish treatment response profiles that can be used to predict efficacy of nitroxoline therapy, we evaluated T_2 and ADC, which are 2 common clinically used MRI parameters. While we found no significant change in T_2 values in the nitroxoline treated group at 7 and 14 days of treatment, there was a significant increase in ADC values after 14 days. Nitroxoline appears to inhibit glioma growth by inducing apoptosis, rather than necrosis, potentially explaining the lack of increased T_2 values in treated tumors. Diffusion MRI has been shown to be highly sensitive to changes in extracellular water content, membrane integrity, and cell density.[24,25] ADC values also correlated with positive treatment outcome.[24,26–31] The small increase in ADC values following nitroxoline treatment observed in our study may reflect the slightly reduced tumor cell density present after treatment-induced apoptosis.

Despite randomized assignment to treatment groups, the nitroxoline-treated group of mice had a significantly larger initial tumor burden (Fig. 5M and N). This fact excludes the possibility that nitroxoline treatment was effective due to a smaller initial tumor burden. Based on our in vitro results, we propose that the cytostatic effect observed in *PTEN/KRAS* gliomas in vivo was due to the ability of nitroxoline to induce G_0/G_1 cell-cycle arrest and lead to apoptosis, as confirmed by the presence of ~15%–20% TUNEL positive nuclei found at histology. While nitroxoline significantly reduced invasion of glioblastoma cells in vitro, we can only speculate about a similar action present in vivo (in *PTEN/KRAS* glioma) due to the inability to distinguish between suppressed growth and/or suppressed invasion using currently available noninvasive imaging techniques.

In summary, we have demonstrated that nitroxoline induces apoptosis, reduces cell invasion, and inhibits glioma growth. Changes in ADC may serve as an imaging biomarker of treatment effect. The history of safe clinical use of nitroxoline as an antimicrobial agent makes this drug a promising candidate for clinical trials for antiglioma therapy.

Supplementary Material

Supplementary material is available online at Neuro-Oncology (http://neuro-oncology.oxfordjournals.org/).

Funding

Intramural funding was provided by the Clinical and Translational Science Institute (CTSI) at the David Geffen School of Medicine at UCLA.

Conflict of interest statement. The corresponding author and all contributing authors do not have any conflict of interest to disclose to Editors-in-Chief, Deputy Editors, Senior Editors, or Scientific Editors, nor do they have any relationships that they believe could be construed as an actual, potential, or perceived conflict of interest with regard to the manuscript submitted for review.

References

1. Johnson DR, O'Neill BP. Glioblastoma survival in the United States before and during the temozolomide era. *J Neurooncol*. 2012; 107(2):359–364.
2. Stupp R, Mason WP, van den Bent MJ, et al. Radiotherapy plus concomitant and adjuvant temozolomide for glioblastoma. *N Engl J Med*. 2005;352(10):987–996.
3. Jiang H, Taggart JE, Zhang X, et al. Nitroxoline (8-hydroxy-5-nitroquinoline) is more a potent anti-cancer agent than clioquinol (5-chloro-7-iodo-8-quinoline). *Cancer Lett*. 2011; 312(1):11–17.
4. Shim JS, Matsui Y, Bhat S, et al. Effect of nitroxoline on angiogenesis and growth of human bladder cancer. *J Natl Cancer Inst*. 2011;102(24):1855–1873.
5. Sosic I, Mirkovic B, Arenz K, et al. Development of new cathepsin B inhibitors: combining bioisosteric replacements and structure-based design to explore the structure-activity relationships of nitroxoline derivatives. *J Med Chem*. 2013;56(2):521–533.
6. Mirkovic B, Renko M, Turk S, et al. Novel mechanism of cathepsin B inhibition by antibiotic nitroxoline and related compounds. *ChemMedChem*. 2011;6(8):1351–1356.
7. Kos J, Lah TT. Cysteine proteinases and their endogenous inhibitors: target proteins for prognosis, diagnosis and therapy in cancer (review). *Oncol Rep*. 1998;5(6):1349–1361.
8. Berdowska I. Cysteine proteases as disease markers. *Clin Chim Acta*. 2004;342(1–2):41–69.
9. Mai J, Sameni M, Mikkelsen T, et al. Degradation of extracellular matrix protein tenascin-C by cathepsin B: an interaction involved in the progression of gliomas. *Biol Chem*. 2002;383(9): 1407–1413.
10. Sobke A, Klinger M, Hermann B, et al. The urinary antibiotic 5-nitro-8-hydroxyquinoline (Nitroxoline) reduces the formation and induces the dispersal of Pseudomonas aeruginosa biofilms by chelation of iron and zinc. *Antimicrob Agents Chemother*. 2012;56(11):6021–6025.
11. de Vries NA, Bruggeman SW, Hulsman D, et al. Rapid and robust transgenic high-grade glioma mouse models for therapy intervention studies. *Clin Cancer Res*. 2010;16(13):3431–3441.
12. Kwon CH, Zhao D, Chen J, et al. Pten haploinsufficiency accelerates formation of high-grade astrocytomas. *Cancer Res*. 2008;68(9): 3286–3294.
13. Huszthy PC, Daphu I, Niclou SP, et al. In vivo models of primary brain tumors: pitfalls and perspectives. *Neuro Oncol*. 2013;14(8): 979–993.
14. Gregorian C, Nakashima J, Le Belle J, et al. Pten deletion in adult neural stem/progenitor cells enhances constitutive neurogenesis. *J Neurosci*. 2009;29(6):1874–1886.
15. Brozovic A, Osmak M. Activation of mitogen-activated protein kinases by cisplatin and their role in cisplatin-resistance. *Cancer Lett*. 2007;251(1):1–16.
16. Guo Y, Yan K, Fang J, et al. Let-7b expression determines response to chemotherapy through the regulation of cyclin D1 in glioblastoma. *J Exp Clin Cancer Res*. 2013;32:41.
17. Plate KH, Breier G, Weich HA, et al. Vascular endothelial growth factor is a potential tumour angiogenesis factor in human gliomas in vivo. *Nature*. 1992;359(6398):845–848.
18. Reardon DA, Wen PY, Desjardins A, et al. Glioblastoma multiforme: an emerging paradigm of anti-VEGF therapy. *Expert Opin Biol Ther*. 2008;8(4):541–553.
19. Li DM, Sun H. PTEN/MMAC1/TEP1 suppresses the tumorigenicity and induces G1 cell cycle arrest in human glioblastoma cells. *Proc Natl Acad Sci USA*. 1998;95(26):15406–15411.
20. Furnari FB, Lin H, Huang HS, et al. Growth suppression of glioma cells by PTEN requires a functional phosphatase catalytic domain. *Proc Natl Acad Sci USA*. 1997;94(23):12479–12484.
21. McCall P, Witton CJ, Grimsley S, et al. Is PTEN loss associated with clinical outcome measures in human prostate cancer? *Br J Cancer*. 2008;99(8):1296–1301.
22. Engelman JA. Targeting PI3 K signalling in cancer: opportunities, challenges and limitations. *Nat Rev Cancer*. 2009;9(8):550–562.
23. Louis DN, Ohgaki H, Wiestler OD, et al. The 2007 WHO classification of tumours of the central nervous system. *Acta Neuropathol*. 2007;114(2):97–109.
24. Chenevert TL, McKeever PE, Ross BD. Monitoring early response of experimental brain tumors to therapy using diffusion magnetic resonance imaging. *Clin Cancer Res*. 1997;3(9):1457–1466.
25. Latour LL, Svoboda K, Mitra PP, et al. Time-dependent diffusion of water in a biological model system. *Proc Natl Acad Sci USA*. 1994; 91(4):1229–1233.
26. Pope WB, Qiao XJ, Kim HJ, et al. Apparent diffusion coefficient histogram analysis stratifies progression-free and overall survival in patients with recurrent GBM treated with bevacizumab: a multi-center study. *J Neurooncol*. 2012;108(3):491–498.
27. Lazovic J, Basu A, Lin HW, et al. Neuroinflammation and both cytotoxic and vasogenic edema are reduced in interleukin-1 type 1 receptor-deficient mice conferring neuroprotection. *Stroke*. 2005;36(10):2226–2231.
28. Hall DE, Moffat BA, Stojanovska J, et al. Therapeutic efficacy of DTI-015 using diffusion magnetic resonance imaging as an early surrogate marker. *Clin Cancer Res*. 2004;10(23):7852–7859.
29. Chenevert TL, Stegman LD, Taylor JM, et al. Diffusion magnetic resonance imaging: an early surrogate marker of therapeutic efficacy in brain tumors. *J Natl Cancer Inst*. 2000;92(24): 2029–2036.
30. McConville P, Hambardzumyan D, Moody JB, et al. Magnetic resonance imaging determination of tumor grade and early response to temozolomide in a genetically engineered mouse model of glioma. *Clin Cancer Res*. 2007;13(10):2897–2904.
31. Pope WB, Kim HJ, Huo J, et al. Recurrent glioblastoma multiforme: ADC histogram analysis predicts response to bevacizumab treatment. *Radiology*. 2009;252(1):182–189.